



## Article

# Long-Term Volumetric Change Estimation of Red Ash Quarry Sites in the Afro-Alpine Ecosystem of Bale Mountains National Park in Ethiopia

Mohammed Ahmed Muhammed <sup>1,2,\*</sup> , Abubeker Mohammed Hassen <sup>3</sup> , Temesgen Alemayehu Abera <sup>1,4</sup> , Luise Wraase <sup>1</sup> , Behailu Legese Ejigu <sup>5</sup> , Binyam Tesfaw Hailu <sup>2,4</sup> , Georg Miehe <sup>6</sup> and Dirk Zeuss <sup>1</sup>

- <sup>1</sup> Department of Environmental Informatics, Faculty of Geography, Philipps-Universität Marburg, Deutschhausstraße 12, 35037 Marburg, Germany; abera@staff.uni-marburg.de (T.A.A.); wraasel@gmail.com (L.W.); dirk.zeuss@uni-marburg.de (D.Z.)
- <sup>2</sup> Remote Sensing and Geo-Informatics Stream, School of Earth Sciences, College of Natural and Computational Science, Addis Ababa University, Addis Ababa P.O. Box 1176, Ethiopia; binyam.tesfaw@aau.edu.et
- <sup>3</sup> Department of Land Administration and Surveying, Center for Geospatial Technology and Land Administration (C-GTLA), Ambo University, Ambo P.O. Box 19, Ethiopia; abubeker.mohammed@ambou.edu.et
- <sup>4</sup> Department of Geosciences and Geography, University of Helsinki, P.O. Box 64 (Gustaf Hällströmin katu 2), FI-00014 Helsinki, Finland
- <sup>5</sup> Department of Geography and Environmental Studies, College of Social Sciences and Humanities, Madda Walabu University, Bale-Robe P.O. Box 247, Ethiopia; behailugisrs@gmail.com
- <sup>6</sup> Department of Geography, Vegetation Geography, Philipps-Universität Marburg, Deutschhausstraße 10, 35037 Marburg, Germany; miehe@staff.uni-marburg.de
- \* Correspondence: mohammed.muhammed@geo.uni-marburg.de or mohammed.ahmedgis@aau.edu.et



**Citation:** Muhammed, M.A.; Hassen, A.M.; Abera, T.A.; Wraase, L.; Ejigu, B.L.; Hailu, B.T.; Miehe, G.; Zeuss, D. Long-Term Volumetric Change Estimation of Red Ash Quarry Sites in the Afro-Alpine Ecosystem of Bale Mountains National Park in Ethiopia. *Remote Sens.* **2024**, *16*, 1226. <https://doi.org/10.3390/rs16071226>

Academic Editors: Hubert Hasenauer, Bogdan Andrei Mihai and Marcel Torok

Received: 5 December 2023  
Revised: 3 March 2024  
Accepted: 24 March 2024  
Published: 30 March 2024



**Copyright:** © 2024 by the authors. Licensee MDPI, Basel, Switzerland. This article is an open access article distributed under the terms and conditions of the Creative Commons Attribution (CC BY) license (<https://creativecommons.org/licenses/by/4.0/>).

**Abstract:** The Bale Mountains National Park (BMNP) in Ethiopia comprises the largest fraction of the Afro-Alpine ecosystem in Africa, which provides vital mountain ecosystem services at local, regional, and global levels. However, the BMNP has been severely threatened by natural and anthropogenic disturbances in recent decades. In particular, landscape alteration due to human activities such as red ash quarrying has become a common practice in the BMNP, which poses a major environmental challenge by severely degrading the Afro-Alpine ecosystem. This study aims to quantify the long-term volumetric changes of two red ash quarry sites in the BMNP using historical aerial photographs and in situ data, and to assess their impact on the Afro-Alpine ecosystem. The Structure-from-Motion multi-view stereo photogrammetry algorithm was used to reconstruct the three-dimensional landscape for the year 1967 and 1984 while spatial interpolation techniques were applied to generate the current digital elevation models for 2023. To quantify the volumetric changes and landscape alteration of the quarry sites, differences in digital elevation models were computed. The result showed that the volume of resources extracted from the BMNP quarry sites increased significantly over the study period from 1984 to 2023 compared with the period from 1967 to 1984. In general, between 1967 and 2023, the total net surface volume of the quarry sites decreased by  $503,721 \pm 27,970 \text{ m}^3$  and  $368,523 \pm 30,003 \text{ m}^3$ , respectively. The extent of the excavated area increased by  $53,147 \text{ m}^2$  and  $45,297 \text{ m}^2$  for Site 1 and 2, respectively. In terms of habitat loss, major gravel road construction inside the BMNP resulted in the reduction of Afro-Alpine vegetation by  $476,860 \text{ m}^2$ , ericaceous vegetation by  $403,806 \text{ m}^2$  and Afromontane forest by  $493,222 \text{ m}^2$  with associated decline in species diversity and density. The excavation and gravel road construction have contributed to the degradation of the Afro-Alpine ecosystem, especially the endemic *Lobelia rhynchopetalum* on the quarry sites and roads. If excavation continues at the same rate as in the last half century, it can threaten the whole mountain ecosystem of the National Park and beyond, highlighting the importance of preventing these anthropogenic changes and conserving the remaining Afro-Alpine ecosystem.

**Keywords:** Afro-Alpine ecosystem; Bale Mountains; digital elevation models; Ethiopia; historical aerial photographs; landscape change

## 1. Introduction

Mountainous ecosystems, except Antarctica, cover nearly 12.3% of the Earth's surface, of which the Alpine zone constitutes about 21.5% or 3.56 million km<sup>2</sup> [1,2]. Among the Alpine ecosystem, the Afro-Alpine zone occurs in tropical Africa above 3200 m elevation and covers 4525 km<sup>2</sup> [3]. The Afro-Alpine ecosystem provides essential ecosystem services at local, regional, and global scales. [4,5]. The Afro-Alpine ecosystem occurs in the scattered high mountains of the East African countries mainly in Ethiopia, Kenya, Tanzania, and Uganda [6,7]. Of these, the Ethiopian Bale Mountains National Park (BMNP), which is registered as one of the United Nations Educational, Scientific and Cultural Organization (UNESCO) World Heritage Sites, is the largest single contiguous Afro-Alpine area in Africa [3]. The BMNP provides a natural habitat to endemic wildlife, and supplies critical water resources to millions of people in the downstream areas [4]. In recent decades, however, the Afro-Alpine ecosystems in BMNP have been severely threatened by climate change and anthropogenic disturbances (e.g., overgrazing, recurrent fires, deforestation, agricultural expansion) mainly driven by rapid population growth [5,8–12]. Of these disturbances, human-induced habitat degradation is the dominant cause [13,14].

Several studies were conducted to assess the degree of land use land cover change in the Afro-Alpine ecosystem [4,5,8,11,15–17]. These studies have reported substantial degradation of forests, grasslands, and shrublands related to agricultural expansion and increased urbanization. However, landscape changes caused by activities such as quarrying and extraction of red ash, which provides much of the key material for paving, road building and related purposes, were not studied in previous studies. Despite the economic benefits of providing building materials and employment opportunities for quarry operators, quarrying affects the natural habitats and ecosystems [18–20].

Quarrying poses a serious environmental threat to the Afro-Alpine ecosystem. It degrades the landscape, affects the physico-chemical properties of the soils, changes groundwater or surface water availability, and negatively affects water quality and salinity [18,21–24]. Moreover, air pollution from quarry dust, blasting, and noise from vehicles and machinery negatively impact animal species and their success in reproduction [23,25].

In BMNP, nearby montane forest and ericaceous belts have been cleared for creating road-access to quarry sites. Such deforestation activity induces warming and affects ecosystem service provision in montane forest [26–29]. Furthermore, deforestation can affect species richness and species diversity in the Afro-Alpine ecosystem like in BMNP, which is one of the East African biodiversity hot spots [4].

For detailed assessment of the historical landscape alterations, such as volumetric change of Afro-Alpine landscape due to quarrying and human-induced land cover change (e.g., from rich and diverse species landscape to bare land) in the BMNP, reliable historical very high spatial resolution orthomosaic aerial images, a Digital Elevation Model (DEM), and efficient mapping methods are required. Such information is important to make evidence-based decisions and for implementing mitigation measures for maintaining sustainability of ecosystem service in the Afro-Alpine ecosystem [10,12,15].

A longer temporal scale of observations is vital to better understand and quantify long-term volumetric changes of landscape alteration in the BMNP and for assessing the effect of quarrying on ecosystem services [30,31]. Historical changes of the landscape can be assessed using geospatial processing of empirical data from Historical Aerial Photographs (HAPs) and maps, satellite imagery, or in situ surveys. Particularly, when historical airborne data are available, time-discrete elevation surfaces can be reconstructed and registered to topographic data for quantitative comparisons [32,33]. HAPs provide valuable information on past landscape conditions, which are useful for mapping, management purpose, and monitoring changes over time [34–36].

The process of reconstructing digital landscape surfaces from HAPs and in situ surveys evolved over time. The traditional aerial triangulations in the early 19th century consumes more time, since manual determination of the optimal initial values for camera poses and 3D points was mandatory [37]. Then, automatic aerial triangulation came later in

1997 to speed up the process [37]. The state of the art for reconstruction of DEM from overlapping HAP images and digital camera images is Structure from Motion Multi-View Stereo photogrammetry, which combines both the photogrammetry and computer vision algorithms [38]. This recent algorithm is user-friendly and particularly well-suited to generating very high-resolution topographic reconstructions [30,39]. However, when reconstructing DEM from in situ field data, different interpolation algorithms could be used, each having its own advantages and disadvantages [40]. The most commonly used methods are inverse distance weighting (IDW), kriging, spline, trend, natural neighbor, generative adversarial networks, and topo-to-raster [41–44].

Quantifying the volumetric change in landscape over a longer time period is essential to assess landform change and evolution [33,45]. Calculating DEMs of Difference (DoD) is the most commonly used technique for quantifying landscape alteration and volumetric changes over time using multi-temporal DEMs [30,33,46–48]. This technique mainly uses cell-by-cell elevation differencing between successive DEMs to produce DoD maps for estimating the net volumetric changes of the topography over a period of time [32,49].

This study aims to estimate, for the first time, the long-term (i.e., >50 years) volumetric landscape changes due to red ash quarrying in the BMNP Afro-Alpine ecosystem and analyze its impact on the mountain ecosystem using HAPs (in 1967 and 1984) and in situ data from 2023. The specific objectives of our study are to: (1) reconstruct DEMs and orthomosaics from the HAPs in 1967 and 1984; (2) generate DEMs for the current year by evaluating interpolation methods based on up-to-date field survey data; (3) estimate the volumetric change of the quarry sites between the years 1967, 1984, and 2023; and (4) discuss their impacts on the Afro-Alpine ecosystem.

## 2. Materials

### 2.1. Study Area

BMNP is located in the southern Highlands of Ethiopia in the Oromia National Regional State (Figure 1). It lies between  $6^{\circ}20'27''$  to  $7^{\circ}51'17''$ N and  $39^{\circ}16'58''$  to  $40^{\circ}04'40''$ E, covering an area of approximately 2200 km<sup>2</sup>. The BMNP was officially established in 1970 and encompasses one of the most extensive high-altitude plateaus (up to 4377 m.a.s.l.), the largest contiguous mountain massif (the area above 3000 m.a.s.l.), and the largest area of Afro-Alpine habitat on the African continent [11,16]. It is a major center of faunal and floral endemism, generates numerous natural processes vital to human existence, and supports an important reservoir of genetic resources. The park can be classified into five vegetation zones: Gaysay valley grasslands in the northern part, dry evergreen montane forest, Afro-Alpine located in the central part of the park, the ericaceous belt that spans most of the escarpment areas, and the Haremma moist montane forest in southern slope of the mountains [22,29,50] (Figure 1). The park has been registered by UNESCO as one of the world's heritage sites in 2023 on the 45th session of the World Heritage Committee, increasing Ethiopia's World Heritage list to 11.

The highlands include Ethiopia's second highest peak, which is Mt. Tullu Dimtu at 4377 m.a.s.l. Three dominant landforms can be observed: the northern slopes from 3000 to 3800 m, the central plateau and peaks at 3800 to 4400 m, and the southern escarpment from 1400 to 3800 m. In this study, two quarry sites located in the central part of the Sanneti Plateau of BMNP were used as research sites to assess and quantify their long-term volumetric changes. The two sites (hereafter, "Site 1" and "Site 2") are used as a major source of red ash with an area of 53,788.91 m<sup>2</sup> and 63,835.68 m<sup>2</sup> as of 2023, respectively (Figure 1).

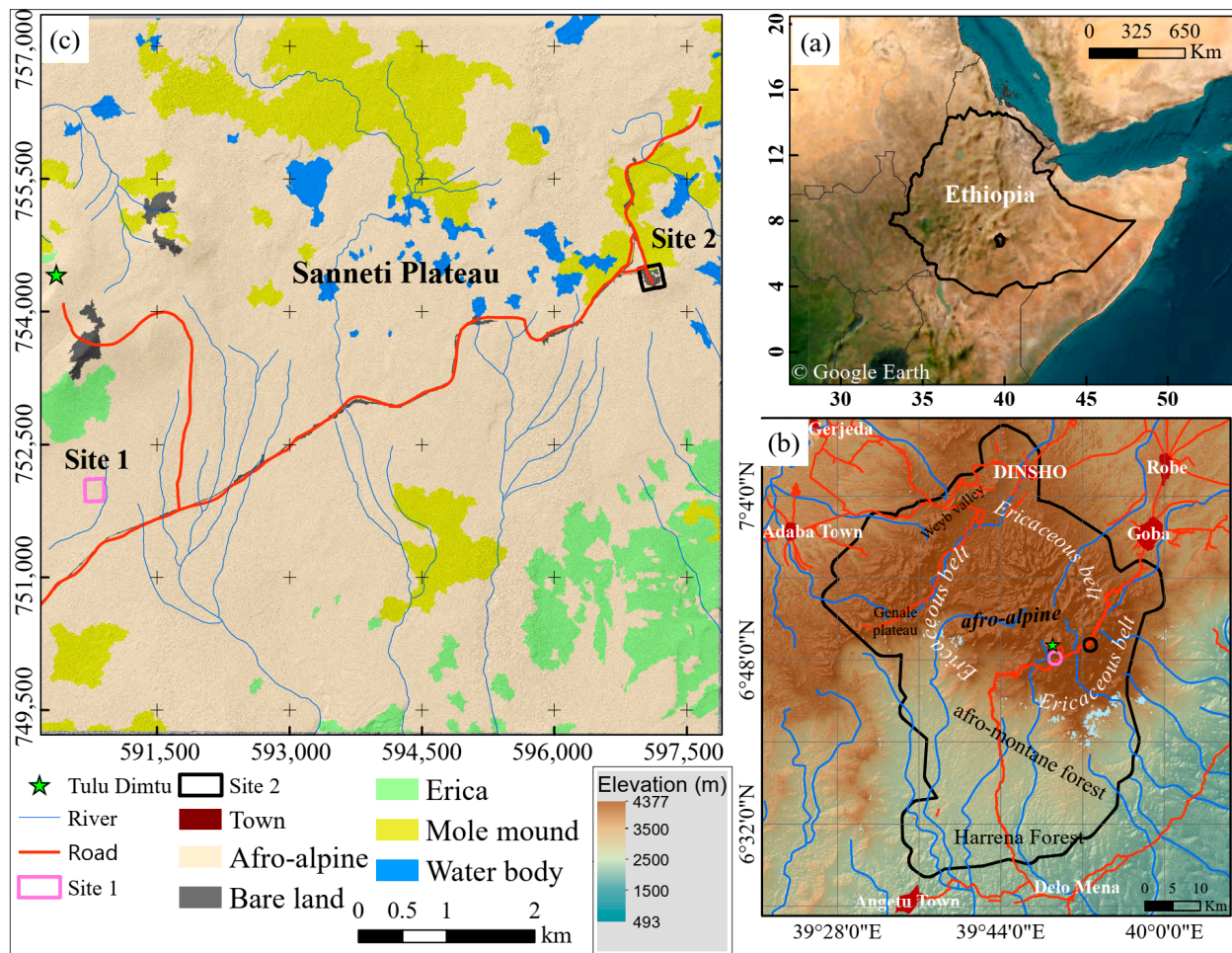


**Figure 1.** Study area in the southern Ethiopian highlands in East Africa with (a) the Bale Mountains National Park (b) and the Sanneti Plateau quarry sites (c). Data: Shuttle Radar Thematic Mapper (United States Geological Survey, Reston, Virginia, USA), Ethio-GIS (Central Statistics Agency, Addis Ababa, Ethiopia), and Georeferenced toposheet (Geospatial Information Institute of Ethiopia, Addis Ababa, Ethiopia) (© Google Earth imagery source: Esri, Maxar, GeoEye, Earthstar Geographics, CNES/Airbus DS, USDA, USGS, AeroGRID, IGN, and the GIS User Community).

## 2.2. Data

In this study, we used HAPs collected on 10 December 1967 and 15–17 January 1984, with approximately 60% and 30% forward and side overlaps, respectively (Figure 2, and Tables 1 and 2). The 1967 HAPs were acquired by the United States Air Force under project number AF 58-3, using a four-engine RC-130A aircraft flying at an altitude of 31,000 feet above terrain equipped with a KC-1(B) PLANIGON camera [51]. This project began in October 1963 to collect visual photography, High Frequency Ranging and Navigation (HIRAN) controlled photography, terrain profile recorder data, HIRAN trilateration, and astronomical and gravimetric survey observations to establish a common geodetic datum of the Ethiopian Empire during the Haile Selassie regime [51]. Similarly, the 1984 HAPs were obtained by the SWEDSURVEY company under project number ET 1:5 using a Wild RC 10 camera (Wild Universal Aviogon II lens type, camera serial number 3045) with an average altitude of 7600 m above terrain [52] (Figure 3, and Tables 3 and 4). The aerial photographs in both projects were taken with a 23 × 23 cm film aerial frame camera and scanned at a resolution of 1200 dots per inch. The quality of all scanned HAPs was checked using Agisoft Metashape professional and found to be well suited for processing with an image quality value above 0.5 pixels.

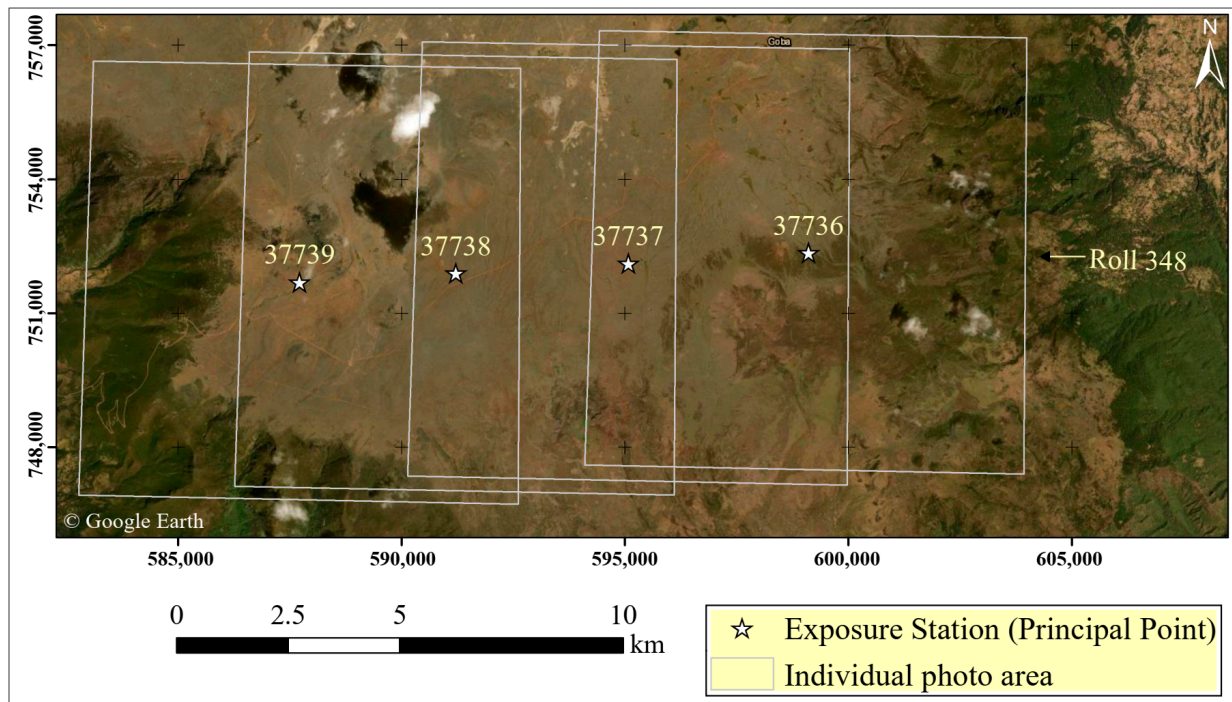


**Figure 2.** Block diagram (flight index) showing camera exposure stations (ground principal points), areal extent and forward overlap of individual aerial photographs for the year 1967 (source: Ethiopian Geospatial Information Institute, and background © Google Earth imagery sources: Esri, Maxar, GeoEye, Earthstar Geographics, CNES/Airbus DS, USDA, USGS, AeroGRID, IGN, and the GIS User Community).

**Table 1.** Flight parameters of historical aerial photographs (HAPs) for the year 1967.

Exposure Date	Calibrated Focal Length (mm)	Flight Height (m)	Overlaps (Forward/Side) (%)	Photo Number
10 December 1967	150.996	9448	60/30	37,736–37,739

**Table 2.** Camera exposure position for the year 1967.

Photo Number	Xo (m)	Yo (m)	Zo (m)
37,736	599,103	752,350	13,437
37,737	595,075	752,119	13,494
37,738	591,208	751,896	13,479
37,739	587,718	751,696	13,373

**Table 3.** Flight parameters of historical aerial photographs (HAPs) for the year 1984.

Exposure Date	Calibrated Focal Length (mm)	Flight Height (m)	Overlaps (Forward/Side) (%)	Photo Number
17 January 1984	152.822	7600	60/30	1657–1658
17 January 1984	152.822	7600	60/30	1618–1622

**Table 4.** Camera exposure positions for the year 1984.

Photo Number	Xo (m)	Yo (m)	Zo (m)
1618	586,452.4576	749,164.9667	10,513.8
1619	590,163.3025	749,468.6249	10,515.7
1620	593,924.6311	749,856.5179	10,516.5
1621	597,799.8222	750,264.2541	10,515.8
1622	602,366.8219	750,870.0517	10,515.1
1657	596,838.6056	758,210.4355	10,526.3
1658	600,708.0729	757,949.1201	10,527.7

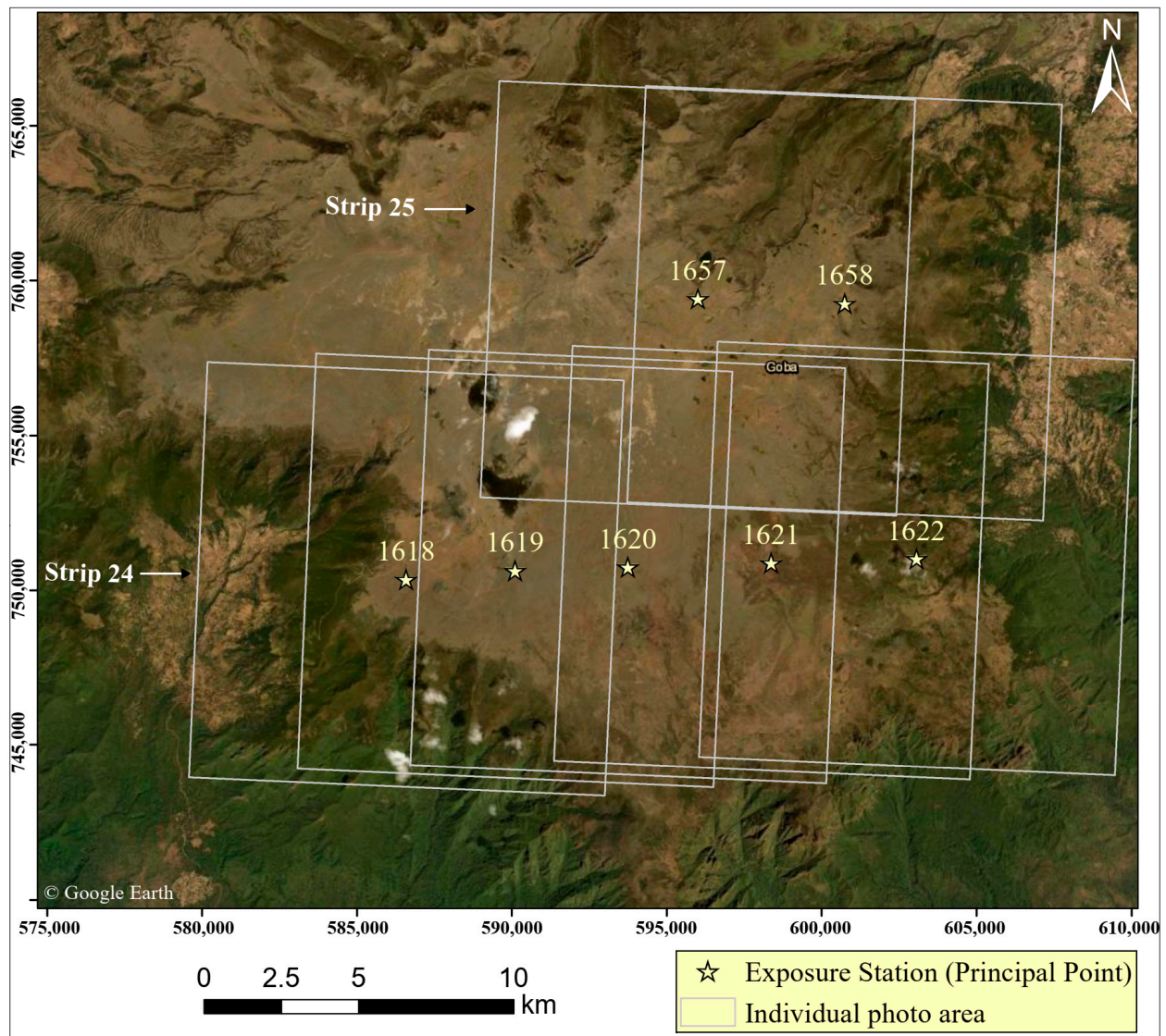


**Figure 3.** Block diagram (flight index) showing camera exposure stations (ground principal points), areal extent, forward overlap, and side overlap of individual aerial photographs for the year 1984 (source: Ethiopian Geospatial Information Institute, and background © Google Earth imagery sources: Esri, Maxar, GeoEye, Earthstar Geographics, CNES/Airbus DS, USDA, USGS, AeroGRID, IGN, and the GIS User Community).

In situ positioning primary data collected using a SOKKIA CX-105 total station were used to generate the current year 2023 DEMs of the study area. A local Geodetic network based on Adindan datum as established by the Ethiopian National geodetic network was used for both historical aerial photograph and in situ survey. In situ surveys are the

most accurate and cost-effective data acquisition method for small project areas and are common for mining projects [53–55]. In most cases, topographic surveying using total stations devices is the most advantageous approach where few high-precision points are required in a relatively enclosed natural topography with breaklines [56]. A total of 308 and 449 topographic points were collected between 25 and 31 May 2023 for Site 1 and Site 2, respectively. From these points, 52 and 90 evenly distributed check points were used for Site 1 and Site 2, respectively, to assess the accuracy of the reconstructed DEMs through spatially interpolated topo points for each quarry site (Figure 4). For data collection, processing, mapping, and related activities, all spatial data were transformed into the Adindan UTM Zone 37 (EPSG: 20137) coordinate system using ArcGIS Desktop version 10.8.2 [57], and all further analyses were performed using the geomorphic change detection software GCDAddIn 7.5.0 [58].

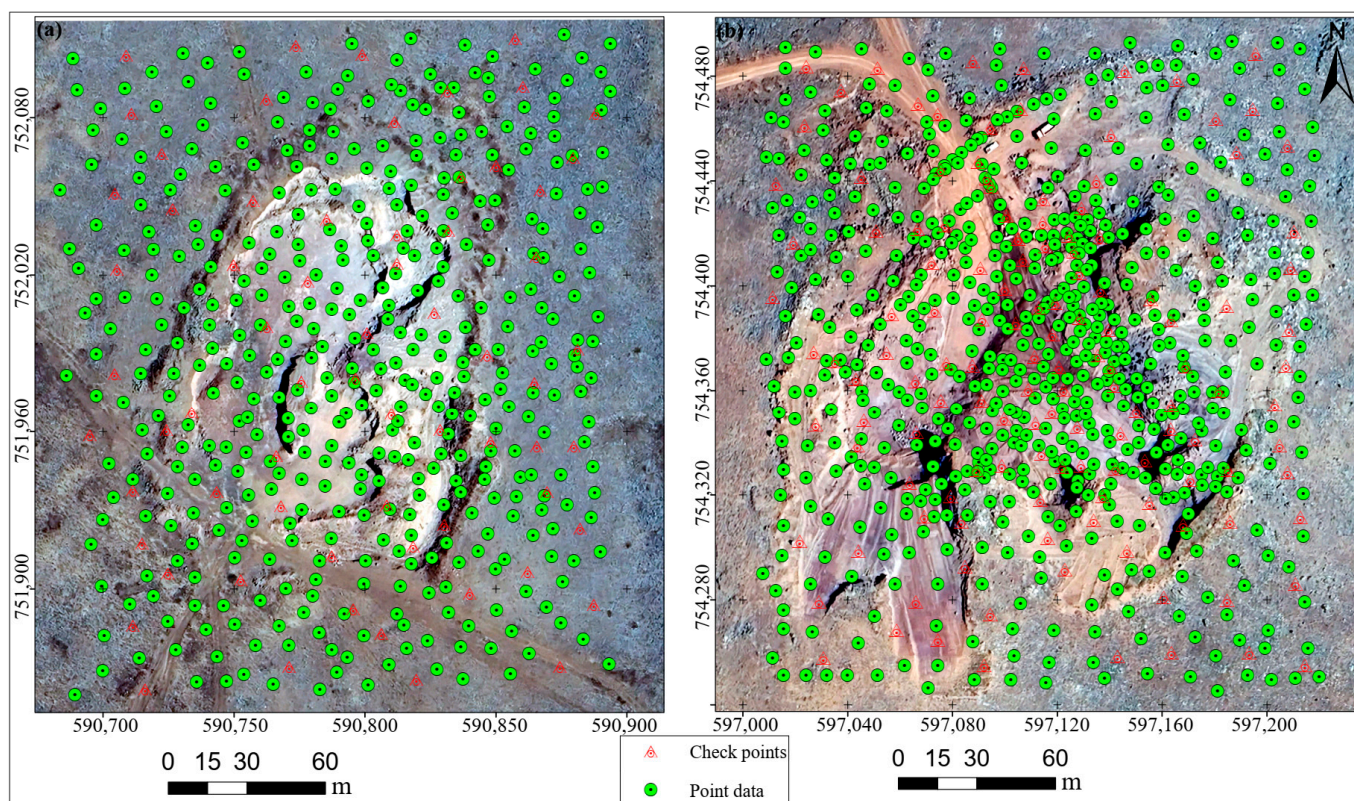


**Figure 4.** Spatial distribution of the in situ primary data collected in the study area for Site 1 (a) and Site 2 (b). The check points (triangle) included in the map were used to assess the accuracy of DEMs generated from point data (Background © Google Earth imagery sources: Esri, Maxar, GeoEye, Earthstar Geographics, CNES/Airbus DS, USDA, USGS, AeroGRID, IGN, and the GIS User Community).

### 3. Methods

#### 3.1. DEMs Generation from HAPs

The Structure-from-Motion Multi View Stereo (SfM-MVS) photogrammetry pipeline was used to reconstruct the three-dimensional structure of the DEM and the orthomosaic from a series of overlapping historical photographs instead of conventional photogrammetry techniques [37]. SfM-MVS photogrammetry is a combination of computer vision and digital photogrammetry, which is preferable because it reduces the working time and resolves the reconstruction of the scene without camera calibration parameters [59]. It is used in a wide range of applications, including archaeology, landscape change assessment, reconstruction of DEMs, and orthomosaic generation [12,60].

We processed 4 and 7 HAPs acquired in 1967 and 1984, respectively, to reconstruct the DEMs for both quarry sites. The processing was performed by assigning appropriate values and settings in the main steps of importing the scanned aerial photographs, aligning the cameras, sparse point cloud generation, optimization, building a dense point cloud and generating the DEMs and orthomosaics for the two quarry sites and for the years 1967 and 1984 using Agisoft Metashape Professional [61] (Figure 5). The quality of the scanned images was checked using Agisoft Metashape professional using the estimate image quality command which all were above 0.5 pixels. After importing the scanned aerial photographs, fiducials, principal points, exposure station coordinates, and inputting fiducial marks, and ground control points (GCPs) (see Supplementary Figures S1 and S2, and Tables S3 and S4), the first step in the process of DEM reconstruction process is alignment which includes aerial triangulation and bundle block adjustment [12]; see Tables 1–4 and Figures 2, 3 and 5. The alignment process started using the Scale Invariant Feature Transform algorithm to generate sparse (tie) point clouds [62]. Then, optimization and camera calibration were done for adjustment of interior and exterior orientation parameters. The depth maps and dense point clouds were generated using sparse (tied) points as input. We used 22 and 30 ground control points for the years of 1967 and 1984, respectively; see Supplementary Tables S1 and S2 for more detail. The final DEMs were generated using dense point clouds as a source of input together with orthomosaics. The accuracy of the DEMs generated for the years 1967 and 1984 were validated by using some of the GCPs as a check point and RMSE value was calculated using Equation (1).

$$\text{Elevation Error} = \sqrt{\frac{1}{N} \sum_{i=1}^N [(Z_{i, est} - Z_{i, in})^2]} \quad (1)$$

where  $i$  is the identification number of each check point ranging from 1 to  $N$ ,  $Z_{i, est}$  is the estimated value,  $Z_{i, in}$  is the observed input (known) value, and  $N$  is the total number of checkpoints.

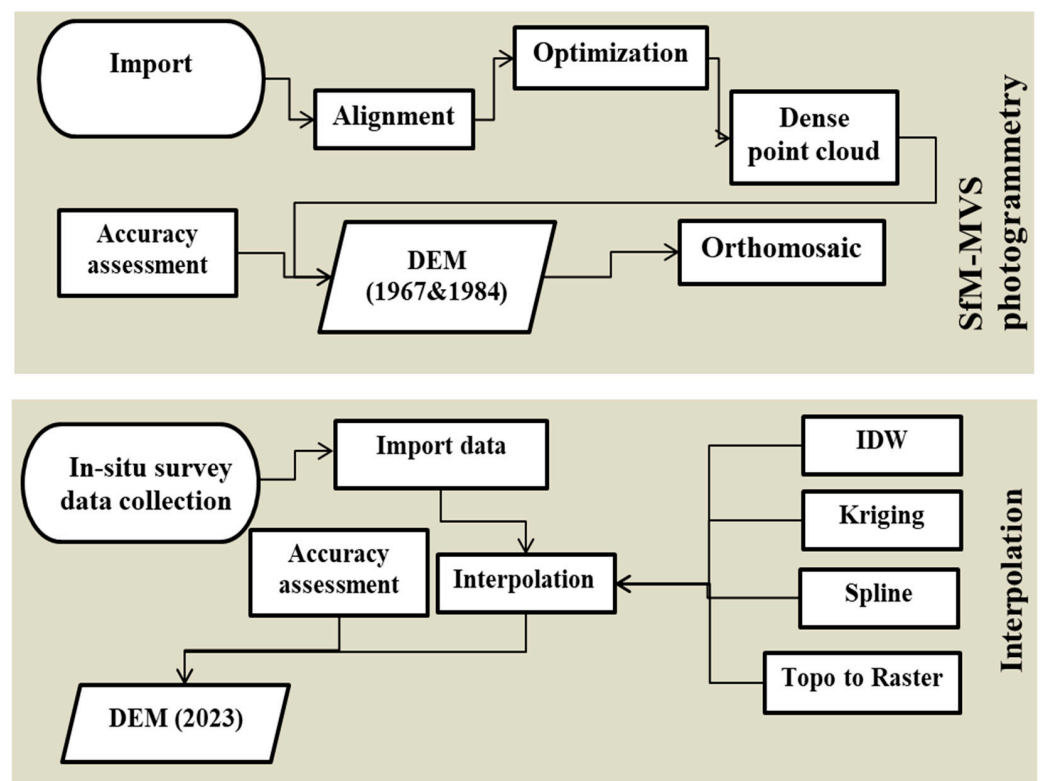
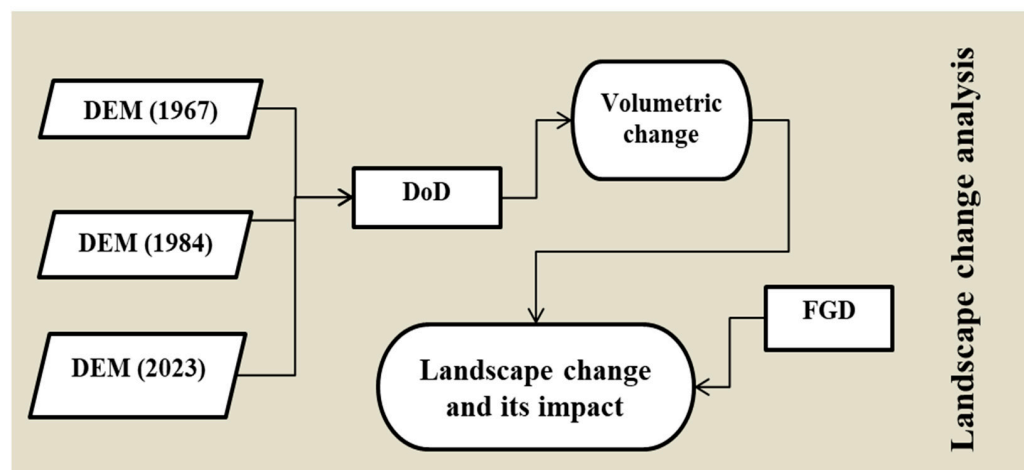


Figure 5. Cont.



**Figure 5.** Methodological workflow applied for landscape volumetric change calculating Digital Elevation Models (DEMs) of Differences (DEMs). SfM MVS = Structure-from-Motion Multi View Stereo photogrammetry, HAPs = Historical Aerial Photographs, IDW = Inverse Distance Weighting, FGD = Focus Group Discussion, DoD = DEM of Difference.

### 3.2. DEMs Interpolation from the In Situ Data for the Year 2023

DEM interpolation was applied to predict the elevation values and to reconstruct the 3D landscape of unobserved locations by providing a series of collected point elevations [41]. Different interpolation methods can produce different results, and each has its own advantages and disadvantages depending on the type of data and topography, despite using the same data source [40,63–65]. Therefore, we examined the most commonly used DEM interpolation methods and assessed their suitability for our study sites and in situ data. In particular, IDW, kriging, spline, and topo-to-raster interpolation techniques were evaluated in this study (Figure 5). The working principles and mathematical issues associated with these interpolation techniques have been described in several previous studies, e.g., [41–44,55,66].

The performance of each interpolation technique was assessed by comparing the RMSE values calculated by determining the difference between the extracted elevations from the estimated surface and the actual values of the in situ point data [67] (Figure 4). In order to compare the DEM interpolation methods and to identify an appropriate one, we evaluated the difference between the known in situ data and the predicted data using the Root Mean Squared Error (RMSE), which indicates the goodness of fit between the actual elevations and the interpolated surface [10,47]. The formula used to calculate the RMSE is Equation (2):

$$RMSE = \sqrt{\frac{1}{N} \sum_{i=1}^N \{z(x_i) - \hat{z}(x_i)\}^2} \quad (2)$$

where  $i$  is the identification number of each check point ranging from 1 to  $N$ ,  $\hat{z}(x_i)$  is the predicted value,  $z(x_i)$  is the observed (known) value, and  $N$  is the total number of checkpoints.

### 3.3. Volumetric Change Estimation and Uncertainties

The DEM of Difference (DoD) mathematical algorithm was applied to the DEMs created from the HAPs and in situ data in order to assess the long-term landscape change and volumetric changes of the quarry sites in the BMNP. The Geomorphic Change Detection 7.5.0 AddIn for ArcMap 10.8.2 was used to create the DoDs and to calculate volumetric changes [68] (Figure 5). It was used to compare the two DEMs, to quantify the net long-term volumetric changes of the two quarry sites in the BMNP due to human-nature interaction, and to produce DoD maps. The DoD maps reveal the areas of sediment loss or accumulation with positive values indicating deposition and negative values indicating areas of loss [10]. Once the two DEMs have been developed and registered to the same grid tessellation, a

DoD was produced by subtracting the earlier DEM from the later DEM on a pixel-by-pixel basis [47] using Equation (3):

$$\Delta E_{ij} = Z_{2ij} - Z_{1ij} \quad (3)$$

where  $\Delta E_{ij}$  is the  $i, j$  grid value of the change in elevation model,  $Z_{1ij}$  is the  $i, j$  value of the early DEM (1967 and 1984), and  $Z_{2ij}$  is the  $i, j$  value of the later DEM (2023). The resulting DoD represents reductions in elevation as negative values and increases in elevation as positive values. This can also reveal the spatial patterns of change based on clusters of cells [68].

The formula below was used for volume difference calculation:

$$V_{diff} = \sum_i a_1^2 \cdot h_i - \sum_j a_2^2 \cdot H_j = a_1^2 \cdot \sum h_i - a_2^2 \cdot \sum H_j \quad (4)$$

$$\frac{\partial V_{diff}}{\partial h_i} = a_1^2 \text{ and } \frac{\partial V_{diff}}{\partial H_j} = a_2^2 \quad (5)$$

where:  $h_i$ —elevation from first DEM;  $H_j$ —elevations from the second DEM;  $a_1$ —resolution of the first DEM; and  $a_2$ —resolution of the second DEM.

The uncertainties in the DEMs were expected to be propagated to the DoD production, and it was therefore essential to identify and minimize errors [33,47]. The total propagated error in the produced DoD can be estimated from the root sum squared errors of the old and new DEM Equations (6) and (7):

$$\delta_{(DoD)} = \sqrt{\delta_{New}^2 + \delta_{Old}^2} \quad (6)$$

where  $\delta_{(DoD)}$  is the propagated error in the DoD, and  $\delta_{New}$  and  $\delta_{Old}$  are the individual errors of the new and old DEMs, respectively.

$$E = \frac{+}{-} (\delta_{DoD} \cdot a_i) \quad (7)$$

where  $E$  is the uncertainty volume,  $\delta_{(DoD)}$  is the propagated elevation error, and  $a_i$  is the area of the study area used for volumetric change analysis (extent of erosion and deposition occurred).

### 3.4. Focus Group Discussion and Interviews

Focus group discussions and key informant interviews were conducted with representatives from the community that are living in the study area for a long time, governmental and non-governmental organizations, experts and managers from the park management office, and local administrators. A mixed questionnaire consisting of both closed and open-ended questions was prepared and distributed to the selected participants. The discussions were conducted using the checklists and discussion guides to get their historical views and perspectives on the impact of red ash excavation on the Afro-Alpine ecosystem and beyond. We integrated both the FGDs and the volumetric change analysis, to determine the landscape change and its impact on the mountain ecosystem (Figure 5).

## 4. Results

### 4.1. DEMs from HAPs and In Situ Data

The 1967 and 1984 DEMs generated from the HAPs for Site 1 and 2 using the Structure-from-Motion Multi View Stereo (SfM-MVS) photogrammetry algorithm are shown in Figure 6. The number of tie points after filtration was 11,072 and 25,534 for the years 1967 and 1984, respectively. These resulted in the generation of dense point clouds of 193,132,444 and 235,285,419 points, respectively. The 1984 tie points and dense point clouds generated were almost doubled compared to that of 1967 due to the number of photographs used. The result showed that the generated DEMs had high accuracy with RMSE values of 0.4 m

and 0.38 m a slightly impacted by flying height, and tie point RMS reprojection errors of 0.22 and 0.09 pixels for the years 1967 and 1984, respectively (Table 5).

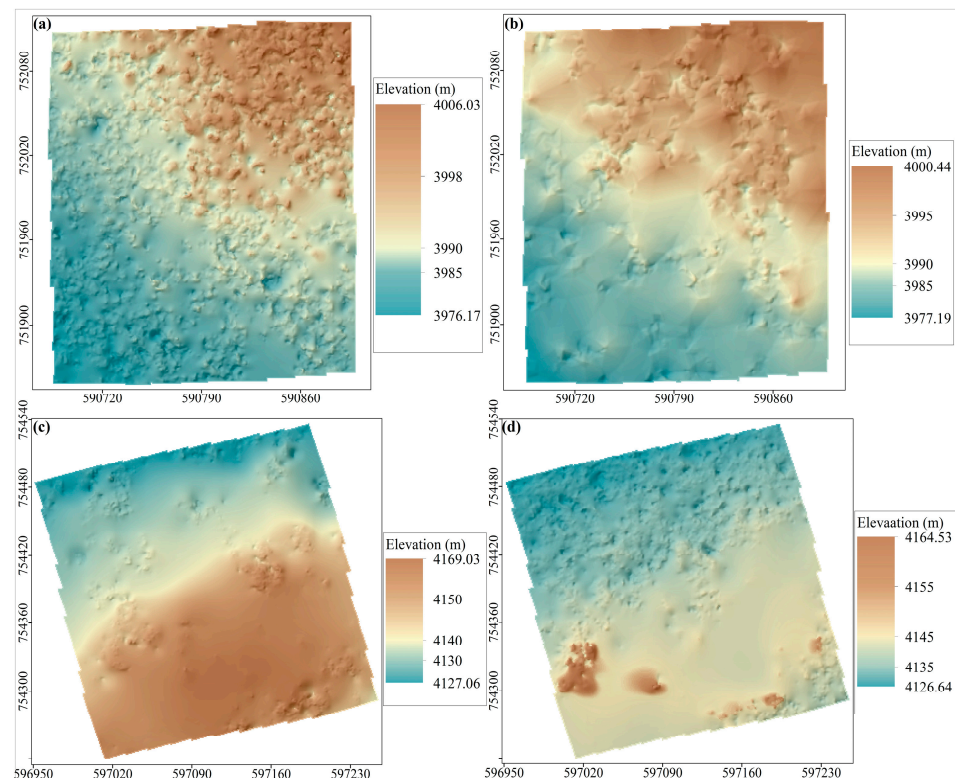


**Figure 6.** DEMs generated from HAPs for Site 1 in 1967 (a) and 1984 (b), and for Site 2 in 1967 (c) and 1984 (d); see also (Figure 1).

**Table 5.** Parameters, processing errors, and final product characteristics used and obtained in HAPs processing.

Specification	1967	1984
Average flight height (m above terrain)	9448	7600
Number of images	4	7
Alignment parameters (accuracy)	Highest	Highest
Depth maps and dense point cloud generation parameters		
Quality	Ultra-high	Ultra-high
Filtering mode	Moderate	Moderate
DEM reconstruction parameters		
Source data	Dense cloud	Dense cloud
Interpolation	Enabled	Enabled
Orthomosaic reconstruction parameters		
Blending mode	Mosaic	Mosaic
Surface	DEM	DEM
Ground sampling distance (m/pix)	0.5	0.5
Number of tie points after filtration	11,072	25,534
Number of dense point clouds	193,132,444	235,285,419
Tie point RMS reprojection error (pix)	0.22	0.09
Average tie point multiplicity	2.04	2.08
Mean key point size	4.00	6.1
Dense cloud point density (point m <sup>-2</sup> )	1.7	1.3
Number of control points	22	30
Total (3D) RMSE (cm) on checkpoints	40.00	38.00

In the 1967 DEM of Site 1, the maximum and minimum elevation of the site was 4006.03 m and 3976.17 m, respectively. However, in the 1984 DEM of the same site, the maximum and minimum elevation was 4000.44 m and 3977.19 m, respectively. Similarly, the 1967 DEM of Site 2 depicts that the highest and lowest elevations were 4169.03 m and 4127.06 m, respectively. However, 4164.53 m and 4126.64 m were also the maximum and minimum elevation in the 1984 DEM of Site 2. The minimum elevation difference was increased by 1 m from 1967 to 1984 for Site 1, in contrast to Site 2. In both quarry sites, there was a noticeable reduction in the elevated topography over time, which in turn reveals a change in the landscape of the area due to the quarrying activities. The direction of red ash extraction was, as expected, towards the uplifted sides. However, there was more change on the central parts (Figures 7–9).

There were noticeable visual differences in elevation between the DEMs generated using different interpolation techniques for both quarry sites. The resulting 2023 reconstructed DEMs for both sites are shown in Figure 7. For Site 1, the maximum elevation was 4000 m asl for both the 1984 and 2023 DEMs, and consequently the difference in the maximum elevation was negligible. However, the difference in elevation minimum was approximately 10 m. The DEM reconstructed using the spline interpolation method for Site 1 had an elevation maximum of 4069 m asl, which is exaggerated by 69 m compared to the actual field data and the resulting DEMs obtained by other interpolation techniques. Similarly, at Site 2, the DEM produced by the spline interpolation method had a maximum elevation difference of 50 m compared to other interpolation methods.

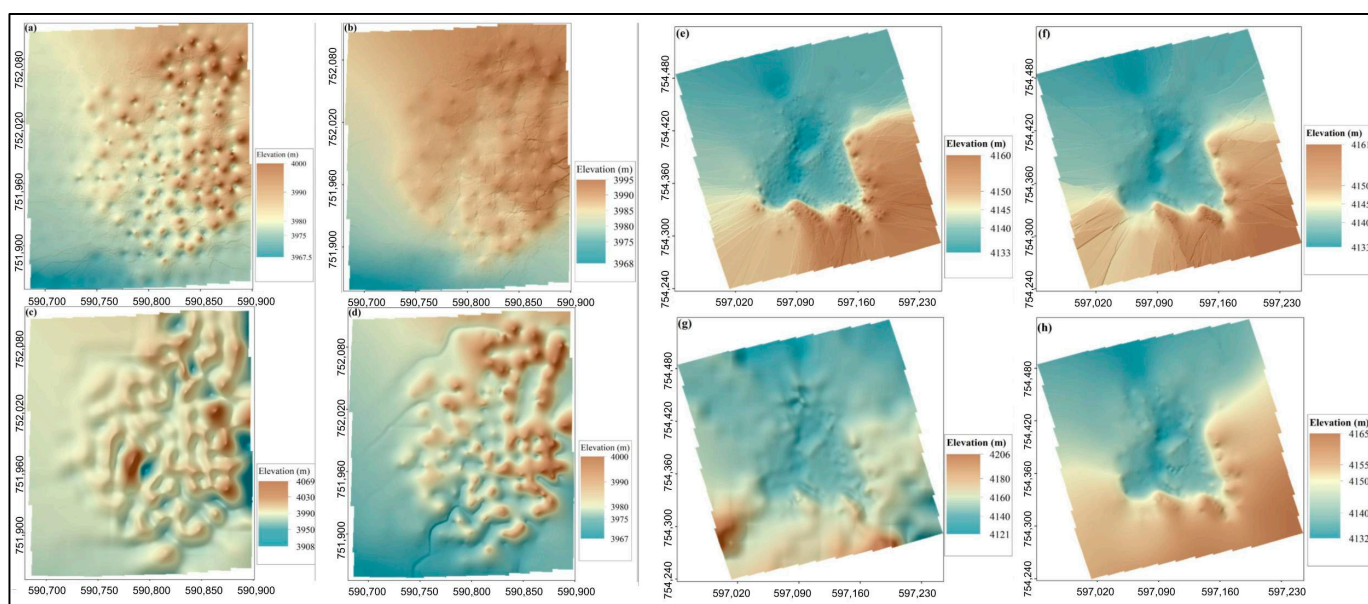


**Figure 7.** DEMs generated from in situ data with different interpolation techniques. Site 1: Inverse Distance Weight (a), kriging (b), spline (c), and topo-to-raster (d). Site 2: Inverse Distance Weight (e), kriging (f), spline (g), and topo-to-raster (h).

The accuracy of the evaluation results of the tested interpolation techniques for both quarry sites are summarized in Table 6. IDW had the best performance for both quarry sites with an RMSE value of 0.360 m and 0.276 m for Site 1 and Site 2, respectively. Following IDW for Site 1 and 2, kriging, topo-to-raster, and spline performed better in chronology. Therefore, the current DEMs for both quarry sites that used to estimate volumetric and landscape changes in this study were generated using the IDW technique, as shown in Figure 7 and Table 6.

**Table 6.** DEM accuracy assessment results of different interpolation techniques for the two quarry sites (in m).

Interpolation Method		IDW	Kriging	Spline	Topo-to-Raster
RMSE	Site 1	0.360	0.751	0.885	0.634
	Site 2	0.276	0.311	0.385	0.381

In the 2023 DEM of Site 1, the maximum and minimum elevations were 4000.18 m and 3967.50 m, respectively. Similarly, 4159.81 m and 4133.39 m were the maximum and minimum elevations of Site 2 (Figure 7). This result shows that the maximum and minimum elevations of the sites were decreasing over the years when compared with the previous DEMs. In addition, there are many large depressions, stockpiles, and quarry wastes that can be visually identified, especially in the quarry of Site 1. Intensive excavation of the red ash material was also observed in the south-western part of Site 2 (Figure 8).

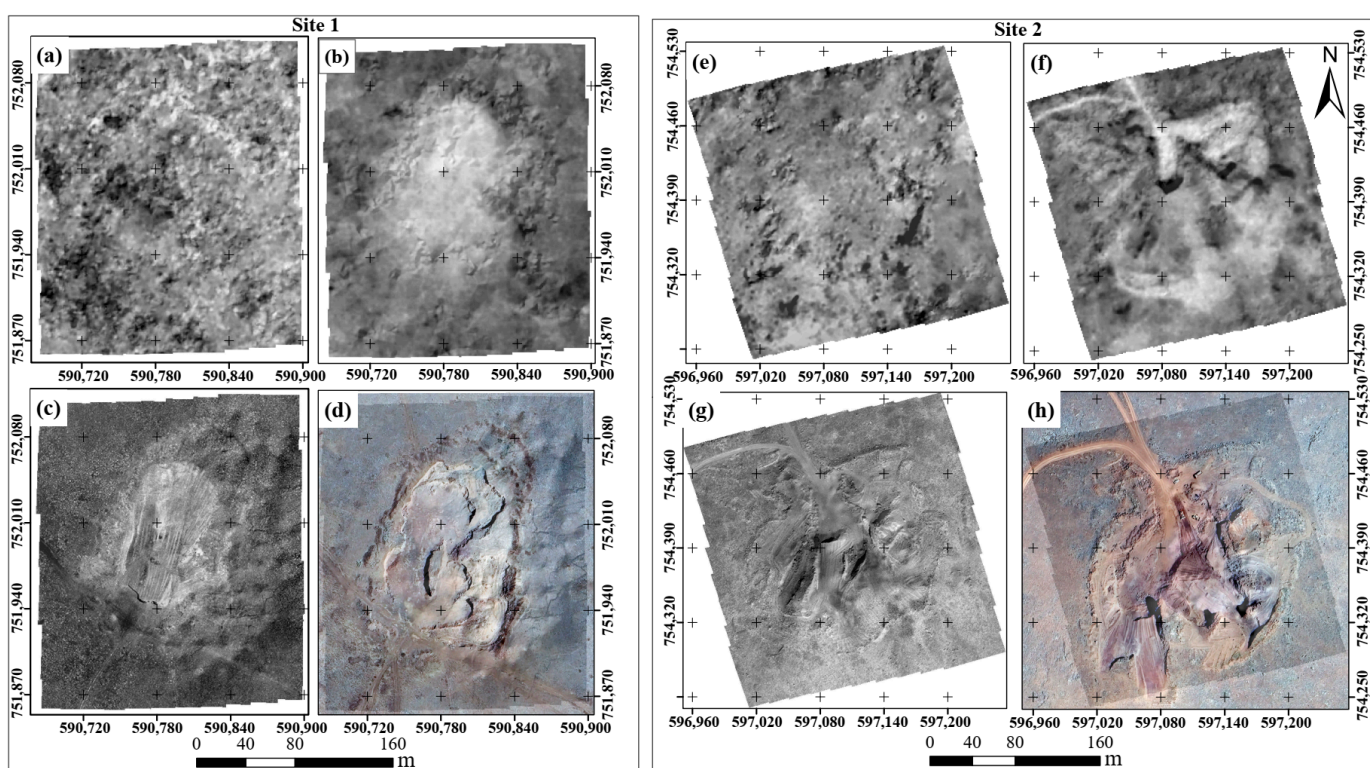


**Figure 8.** Historical aerial images of the two study quarry sites. Historical view of Site 1 in 1967 (a), 1984 (b), 2011 (c), and 2023 (d); and Site 2 in 1967 (e), 1984 (f), 2011 (g), and 2023 (h). (Source: [69]; © Google Earth imagery; Esri, Maxar, GeoEye, Earthstar Geographics, CNES/Airbus DS, USDA, USGS, AeroGRID, IGN, and the GIS User Community).

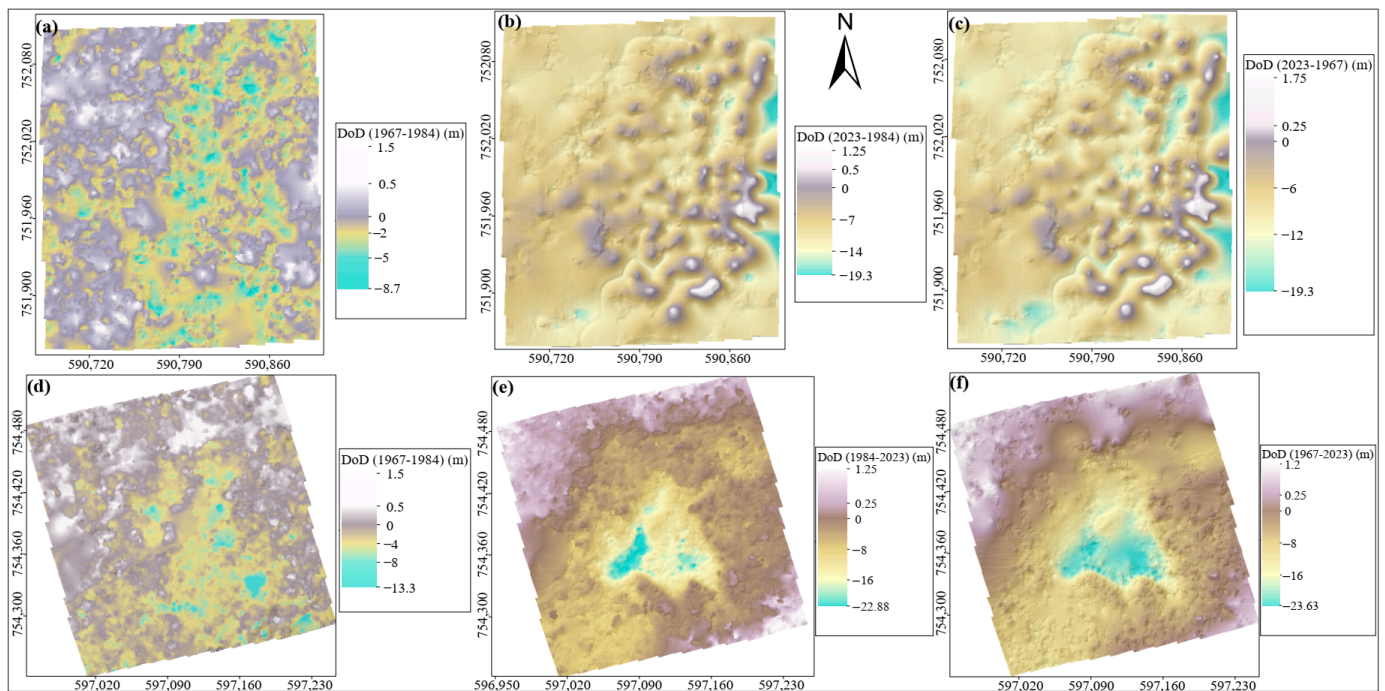


**Figure 9.** DEM of Difference (DoD) in meter showing maps of Site 1 from 1967 to 1984 (a), from 1984 to 2023 (b), and from 1967 to 2023 as a whole (c); and of Site 2 from 1967 to 1984 (d), from 1984 to 2023 (e), and from 1967 to 2023 as a whole (f).

#### 4.2. Volumetric and Landscape Changes

The resulting volumetric and landscape changes show the total volume of surface lowering and rising and the total net volume differences of the quarry sites plus the uncertainty value of each volumetric change (Table 7). Accordingly, the volume of erosion and deposition of the quarry Site 1 were estimated to be  $68,020 \text{ m}^3$  and  $1077 \text{ m}^3$ , respectively for the period December 1967 to January 1984, indicating that the total net volume change of excavation was  $-66,943 \text{ m}^3$  with an uncertainty volume of  $\pm 10,526 \text{ m}^3$ . From January 1984 to May 2023 the volume of erosion and deposition was  $439,399 \text{ m}^3$  and  $2622 \text{ m}^3$  resulting in a total net volume change of excavation of  $-436,777 \text{ m}^3$  with an uncertainty volume of  $\pm 26,894 \text{ m}^3$ . The total net volume change of Site 1 from December 1967 to May 2023 for the last 56 years was  $503,721 (\pm 27,970 \text{ m}^3)$ . Similarly,  $104,892 \text{ m}^3$  and  $1033 \text{ m}^3$  were recorded as the volume of erosion and deposition of Site 2 from December 1967 to January 1984, respectively, indicated that the total net volume change of excavation was  $-103,859 \text{ m}^3$  with an uncertainty volume of  $\pm 12,784 \text{ m}^3$ . From January 1984 to May 2023,  $267,507 \text{ m}^3$  and  $2842 \text{ m}^3$  were the volume of erosion and deposition, respectively, and  $-264,664 \text{ m}^3$  was the total estimated net volume change of Site 2 with an uncertainty volume of  $\pm 28,726 \text{ m}^3$ . Thus, significant volumes of excavation were recorded at both quarry sites, although more at Site 1 than at Site 2. A total of  $872,244 \text{ m}^3$  has been extracted from both quarry sites in the Afro-Alpine ecosystem of the Sanetti plateau over the last 56 years.

In addition to calculating the amount of landscape volumetric change, the physical 2D change of the two sites in four years is shown in Figure 8.

The obtained DoD from 1967 to 1984, 1984 to 2023, and from 1967 to 2023 of excavation and deposition ranges from  $-23.63 \text{ m}$  to  $1.75 \text{ m}$ . Specifically, the excavated DoD values were  $-8.7$  and  $-13.3$  from 1967 to 1984 for Site 1 and Site 2, respectively. However, from 1984 to 2023, the excavated height value almost doubled for Site 1 ( $-19.3 \text{ m}$ ) and Site 2 ( $-22.88 \text{ m}$ ), respectively (Figure 9).

**Table 7.** Total volume of surface lowering, total volume of surface raising, and total net volumetric ( $\text{m}^3$ ) changes with uncertainty volume of the quarry sites.

Site	Change Period	Total Volume of Surface Lowering	Total Volume of Surface Raising	Total Net Volume Change
1	December 1967–January 1984	68,020	1077	−66,943 ( $\pm 10,526$ )
	January 1984–May 2023	439,399	2622	−436,777 ( $\pm 26,894$ )
	December 1967–May 2023	507,420	3699	−503,721 ( $\pm 27,970$ )
2	December 1967–January 1984	104,892	1033	−103,859 ( $\pm 12,784$ )
	January 1984–May 2023	267,507	2842	−264,664 ( $\pm 28,726$ )
	December 1967–May 2023	372,399	3876	−368,523 ( $\pm 30,003$ )

## 5. Discussion

### 5.1. DEM Reconstruction and Interpolation

In recent decades, numerous studies were conducted to explore the potential link between the human–nature relationship and its impact on the environment. Longer temporal scale observations are an essential approach to better understand and quantify these complex interactions and their impacts using HAPs and current in situ data [12,47]. Therefore, the DEMs of the historic landscape were reconstructed using SfM-MVS photogrammetry and interpolation algorithms. However, the accuracy of DEMs generated from historical aerial photography is affected by flight height. Thus, we have improved the accuracy by incorporating input parameters (focal length, principal point coordinates, affinity and skew transformation coefficients, radial distortion coefficients, and tangential distortion coefficients) and using very high accuracy and more GCPs following similar approaches in previous studies [30,70–72]. The accuracy of the DEMs generated for the years 1967 and 1984 is 0.4 m and 0.38 m, respectively. A previous study elsewhere [72] also achieved an accuracy of 0.4 m and 0.22 m using 25 and 50 GCPs, respectively, for the reconstruction of historical DEMs flown at extremely high altitudes.

We also investigated the four most commonly used interpolation techniques (IDW, kriging, spline, and topo-to-raster) to generate DEMs from the in situ point data. Various factors such as the nature of the terrain, the distribution of the sampling points, and the surveying methods used with the interpolation techniques have a great influence on the accuracy of DEMs [40,64,65]. For example, spline [65], kriging [40], topo-to-raster [64], and IDW [44,64,73] all gave good results as reported in these studies. However, when compared to other methods in our context and supplemented by [64,65], the results of our study showed that the IDW interpolation method produced the best fitting DEMs for both quarry sites. Kriging was only the second best interpolation method for both quarry sites, which stands in contrast to other comparative assessment studies carried out so far, in which kriging was the best performing interpolation method [40,74].

### 5.2. Landscape Volumetric Change and Uncertainties

The volume of extracted resources in the quarry sites of the BMNP in the Sanneti plateau mountain ecosystem significantly increased over the study period (Table 7; Figures 8 and 9). The amount of red ash excavated during the period from 1984 to 2023 was three to six times higher than the amount of red ash excavated during the period from 1967 to 1984. This was likely due to the excavation that started during the construction of the gravel road that crosses the Sanneti plateau from the towns of Goba to Harena Bulluk through Rira and Delo Mena. This road was constructed in the 1970's during the Ethio-Somali war and the establishment of the Shawe military camp base and its maintenance continuously needs building material. In general, from 1967 to 2023,  $-503,721 (\pm 27,970) \text{ m}^3$  and  $-368,523 (\pm 30,003) \text{ m}^3$  were recorded as the total net surface volume changes of quarry Site 1 and Site 2, respectively. In both sites, the values of volumetric change were highly negative, which illustrates that the landscape changes in these areas are extremely altered by excavation and human interference. This result is in line with previous studies in

BMNP [4,5,8,15–17], which have shown that anthropogenic factors played and still play a major role in the degradation of the Afro-Alpine ecosystem.

### 5.3. Major Causes and Drivers of Red Ash Excavation and Its Environmental Impact

Potential triggers for red ash extraction from the Afro-Alpine ecosystem of BMNP, identified through focus group discussions, include: (1) demand for cost-effective material, (2) unavailability of alternative materials around, and (3) lax law enforcement. Among the three most important factors, the demand for low-cost effective material is chosen as the first reason for the excavation of the mountain, given priority by 75% of the respondents. The selection of quarry sites was strategic, considering their proximity to areas requiring construction materials, particularly neighboring Woredas like Goba, Delo Mena, and Harena Bulluk. The primary beneficiary of excavated material is a governmental office, notably the Ethiopian Rural Road Authority, impacting both the environment and local communities. The excavated material likely contributes to road construction, such as the Goba to Harena Bulluk route through BMNP, altering the landscape significantly without compensation (Figure 1).

Findings from discussions and interviews reveal two primary ways in which red ash excavation affects vegetation. Firstly, the quarrying process itself removes vegetation, expanding the excavated area up to 53,147 m<sup>2</sup> and 45,297 m<sup>2</sup> for Site 1 and 2, respectively. Secondly, quarrying leads to the creation of secondary tracks or roads, damaging additional vegetation. For example, Afro-Alpine vegetation of 476,860 m<sup>2</sup>, ericaceous vegetation of 403,806 m<sup>2</sup>, and Harena forest of 493,222 m<sup>2</sup> were removed on the way from Goba to Delo Mena due to a single major gravel road construction inside the BMNP. The use of heavy machinery in excavation, transportation, and road construction contributes to significant vegetation loss and soil erosion (Figure 8h, Site 2). Up to ten truckloads are transported daily, leading to bare soil exposure, erosion, altered topography, and changes in drainage patterns, making vulnerable areas susceptible to flooding (Figures 10 and 11).

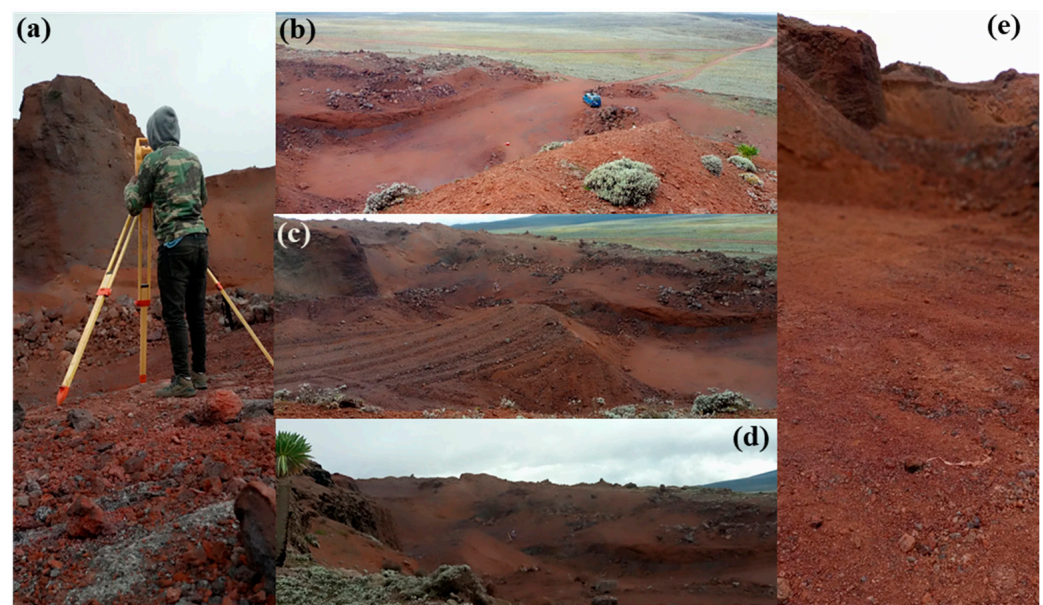


**Figure 10.** Topographic data collection using a total station and documented landscape change due to quarrying operations in the BMNP. (a) Collecting data using a total station, (b) newly formed road entry to the site, (c,d) excavated surfaces vulnerable to flooding, and (e) cliff formation prone to further erosion (Photo: B. Bekelle).

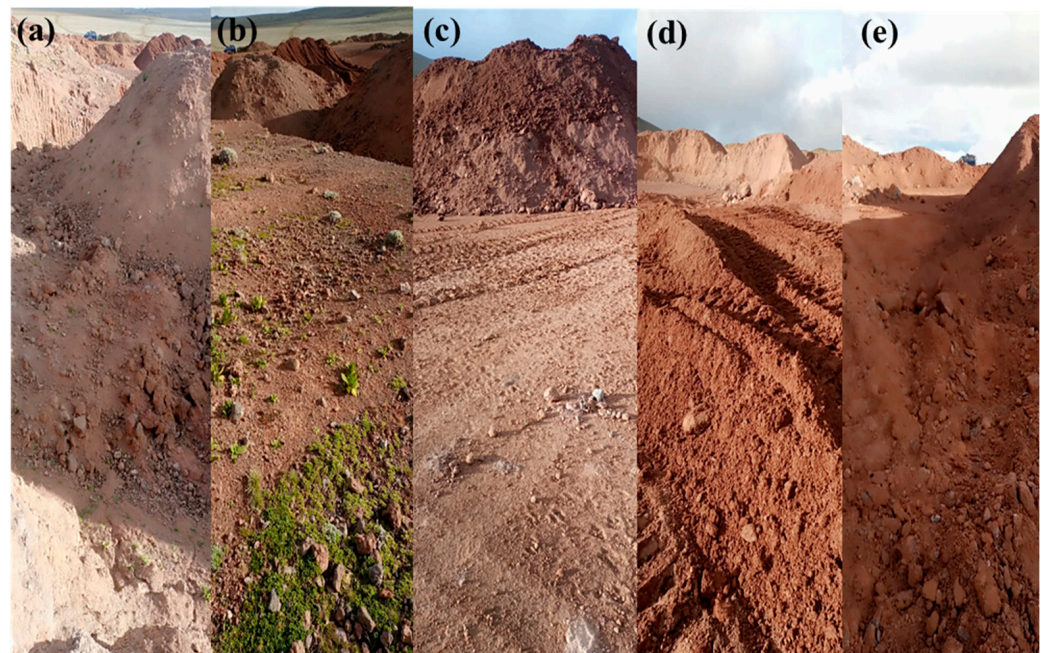


**Figure 11.** Landscape change due to quarrying operations in the BMNP. (a,e) Newly formed drainage pattern, (b) excavated surfaces, (c) stockpile, and (d) machine and vehicle footprint (Photo: B. Bekelle).

Quarrying activities likely impact the physical, chemical, and biological components of soil resources, increasing the risk of erosion. Removal of protective layers exposes rocks and lower layers, mirroring challenges reported in related studies [19]. Excavated areas, stockpiles, and quarry waste negatively impact landscape form, affecting the visual appeal of BMNP. Excavation leaves depressions forming potential hazardous ponds, particularly in the summer season [75] (Figure 10).

Focus group discussions highlight residents' observations regarding landscape change, land degradation, and deforestation of Afro-Alpine vegetation. Afro-Alpine species that are being degraded include for example, species of *Helichrysum* (*H. splendidum*, *H. citrispinum*, *H. cymosum*, *H. jormosissimum*), species of *Alchemilla*, *Festuca abyssinica*, *Erica trimera* and *Erica Arboria*, and especially the endemic *Lobelia rhynchopetalum* (see Supplementary Figure S3 and Table S5). They also observed a decrease in species diversity, air, water and noise pollution, cave and sinkhole formation, damage to biodiversity, terrestrial ecosystem degradation, water resource depletion, and improper quarry waste disposal. Continued excavation poses threats to tree and vegetation species, with road maintenance impacting biodiversity indirectly through noise, vibration, clearing for machinery access, material and waste stockpiles, soil disturbance, runoff, wastewater disposal, artificial lighting, and increased human activity. These cumulative impacts may disturb animal species within the park, emphasizing the urgent need for mitigation measures to preserve the delicate ecosystem of BMNP (Figures 10 and 11).

## 6. Conclusions

Although the Bale Mountains are home to a large number of fauna and flora endemisms, they have experienced changes over the last half century due to continued excavation. The volumetric change analysis carried out and verified in the field clearly shows that the Afro-Alpine landscape, one of the mountain ecosystems, which provides important ecological and ecosystem services in the tropics, is threatened by human activities in the region. In this study, we used HAPs and in situ data in the Afro-Alpine ecosystem of BMNP, the second-highest location in Ethiopia. Employing a recently developed Structure from Motion-Multi View Stereo photogrammetry method, we reconstructed the landscapes of 1967 and 1984, generating DEMs and orthomosaics. For the current landscape in 2023, we tested four interpolation methods IDW, kriging, spline, and topo-to-raster, and selected

the IDW method due to its superior accuracy compared to the other methods. The accuracy of the generated DEMs was 0.40 m and 0.38 m for the year 1967 and 1984, respectively; while 2023 DEMs achieved an accuracy of 0.360 m and 0.276 m for Site 1 and Site 2.

The reconstructed DEMs for 1967, 1984, and 2023 were used to conduct an in-depth analysis of the long-term red ash excavation volumes from both sites by calculating DEMs of differences and associated uncertainties. Our findings showed that approximately 872,244 m<sup>3</sup> of red ash material has been excavated from the BMNP quarries since 1967, with uncertainties up to  $\pm 30,003$  m<sup>3</sup>. Since the 1970s, the excavation process in BMNP has also adversely impacted the Afro-Alpine ecosystem by removing the vegetation cover causing a reduction of ericaceous and Afromontane forest by 403,806 m<sup>2</sup> and by 493,222 m<sup>2</sup>, respectively. Our result indicated that red ash excavation over the last half century has considerably altered the vegetation cover of mountain ecosystems through reducing the extent of ericaceous and Afromontane forest.

If quarrying continues at the current rate, it may pose a serious threat to the entire mountain ecosystem of the BMNP. Our results provide valuable insights for the scientific community and natural resource managers, facilitating an understanding of the need for mitigation measures to reduce the adverse impacts of excavation on the Afro-Alpine ecosystem.

**Supplementary Materials:** The following supporting information can be downloaded at: <https://www.mdpi.com/article/10.3390/rs16071226/s1>. Ref. [76] is cited in the Supplementary materials.

**Author Contributions:** Conceptualization, M.A.M., L.W., D.Z., and G.M.; methodology, M.A.M., D.Z., and A.M.H.; validation, M.A.M., D.Z., and A.M.H.; formal analysis, M.A.M. and A.M.H.; resources, M.A.M. and B.L.E.; data curation, M.A.M. and B.L.E.; writing—original draft preparation, M.A.M., and A.M.H.; writing—review and editing, M.A.M., A.M.H., L.W., T.A.A., and D.Z.; visualization, M.A.M.; supervision, T.A.A., B.T.H., G.M., and D.Z.; funding acquisition, G.M. and. All authors have read and agreed to the published version of the manuscript.

**Funding:** This work was supported by Deutsche Forschungsgemeinschaft (DFG) Award no. NA 783/12-1, AOBJ 628803 through a project entitled “The mountain exile hypothesis: how humans benefited from and re-shaped African high-altitude ecosystems during Quaternary climatic changes” within the framework of Research Unit 2358.

**Data Availability Statement:** The raw data supporting the conclusions of this article will be made available by the authors on request.

**Acknowledgments:** This research was funded by the German Research Council (DFG) in the framework of the joint Ethio-European Research Unit 2358 “The Mountain Exile Hypothesis: how humans benefited from and re-shaped African high-altitude ecosystems during Quaternary climatic changes”. We thank the Geospatial Information Institute of Ethiopia for provided us the necessary data and documents; and Ethiopian Wildlife Conservation Authority, the Philipps University of Marburg, the Ethiopian Wolf Project, and the Bale Mountains National Park for their cooperation and permission to conduct field work. We also very much appreciate the support of Belayneh Bekelle, Mohammed Kedir, Hussein, Gash Kasim, Awol Assefa, Sofia, Wege Abebe, and Katinka Thielsen, without whom it would not have been possible to do the field work in the Bale Mountains. We thank Spaska Forteva for her help in arranging lab facilities. We also would like to acknowledge the anonymous reviewers.

**Conflicts of Interest:** The authors declare no conflicts of interest. The funders had no role in the design of the study; in the collection, analyses, or interpretation of data; in the writing of the manuscript; or in the decision to publish the results.

## References

1. Testolin, R.; Attorre, F.; Jiménez-Alfaro, B. Global Distribution and Bioclimatic Characterization of Alpine Biomes. *Ecography* **2020**, *43*, 779–788. [[CrossRef](#)]
2. Körner, C. *Alpine Plant Life: Functional Plant Ecology of High Mountain Ecosystems*, 3rd ed.; Springer: Cham, Switzerland, 2021; ISBN 978-3-030-59537-1.
3. de Deus Vidal, J.; Clark, V.R. Afro-Alpine Plant Diversity in the Tropical Mountains of Africa. In *Encyclopedia of the World's Biomes*; Elsevier: Amsterdam, The Netherlands, 2020; pp. 373–394. ISBN 978-0-12-816097-8.

4. Chignell, S.M.; Laituri, M.J.; Young, N.E.; Evangelista, P.H. Afroalpine Wetlands of the Bale Mountains, Ethiopia: Distribution, Dynamics, and Conceptual Flow Model. *Ann. Am. Assoc. Geogr.* **2019**, *109*, 791–811. [[CrossRef](#)]
5. Teshome, A.; Randall, D.; Kinahan. The Changing Face of the Bale Mountains National Park over 32 Years: A Study of Land Cover Change. In *Walia Journal of the Ethiopian Wildlife and Natural History Society*; Ethiopian Wildlife and Natural History Society: Addis Ababa, Ethiopia, 2011; Volume 2011, pp. 118–130. ISBN 0083-7059.
6. Fetene, A.; Alem, D.; Mamo, Y. Effects of Landuse and Land Cover Changes on the Extent and Distribution of Afroalpine Vegetation of Northern Western Ethiopia: The Case of Choke Mountains. *Res. J. Environ. Sci.* **2014**, *8*, 17–28. [[CrossRef](#)]
7. Kebede, M.; Ehrlich, D.; Taberlet, P.; Nemomissa, S.; Brochmann, C. Phylogeography and Conservation Genetics of a Giant Lobelia (*Lobelia Giberroa*) in Ethiopian and Tropical East African Mountains. *Phylogeography A Giant Lobelia Mol. Ecol.* **2007**, *16*, 1233–1243. [[CrossRef](#)] [[PubMed](#)]
8. Abdissa, G. *Ecosystem Viability Assessment and Fragmentation Analysis in Bale Mountains National Park (Emphasis on Afro-Alpine Ecosystem)*; Addis Ababa University: Addis Ababa, Ethiopia, 2010.
9. Gashaw, T. Threats of Bale Mountains National Park and Solutions, Ethiopia. *J. Phys. Sci. Environ. Stud.* **2015**, *1*, 10–16.
10. Nourbakhshbeidokhti, S.; Kinoshita, A.; Chin, A.; Florsheim, J. A Workflow to Estimate Topographic and Volumetric Changes and Errors in Channel Sedimentation after Disturbance. *Remote Sensing* **2019**, *11*, 586. [[CrossRef](#)]
11. Muhammed, A.; Elias, E. Class and Landscape Level Habitat Fragmentation Analysis in the Bale Mountains National Park, Southeastern Ethiopia. *Heliyon* **2021**, *7*, e07642. [[CrossRef](#)]
12. Muhammed, M.A.; Hailu, B.T.; Mieke, G.; Wraase, L.; Nauss, T.; Zeuss, D. High-Resolution Digital Elevation Models and Orthomosaics Generated from Historical Aerial Photographs (since the 1960s) of the Bale Mountains in Ethiopia. *Earth Syst. Sci. Data* **2023**, *15*, 5535–5552. [[CrossRef](#)]
13. Vitousek, P.M.; Mooney, H.A.; Lubchenco, J.; Melillo, J.M. Human Domination of Earth's Ecosystems. In *Urban Ecology*; Marzluff, J.M., Shulenberg, E., Endlicher, W., Alberti, M., Bradley, G., Ryan, C., Simon, U., ZumBrunnen, C., Eds.; Springer: Boston, MA, USA, 2008; pp. 3–13. ISBN 978-0-387-73411-8.
14. Muhammed, A.; Elias, E. The Effects of Landscape Change on Plant Diversity and Structure in the Bale Mountains National Park, Southeastern Ethiopia. *Int. J. Ecol.* **2021**, *2021*, 1–13. [[CrossRef](#)]
15. Desta, W.A. *Assessment of Land Use Land Cover Dynamics at Bale Mountains National Park Using Gis and Remote Sensing*; Addis Ababa University: Addis Ababa, Ethiopia, 2007.
16. Kidane, Y.; Stahlmann, R.; Beierkuhnlein, C. Vegetation Dynamics, and Land Use and Land Cover Change in the Bale Mountains, Ethiopia. *Environ. Monit. Assess.* **2012**, *184*, 7473–7489. [[CrossRef](#)]
17. Hailemariam, S.; Soromessa, T.; Teketay, D. Land Use and Land Cover Change in the Bale Mountain Eco-Region of Ethiopia during 1985 to 2015. *Land* **2016**, *5*, 41. [[CrossRef](#)]
18. Endalew, A.; Tasew, E.; Tolahun, S. Environment and Social Impacts of Stone Quarrying: South Western Ethiopia, in Case of Bahir Dar Zuria Wereda Zenzelma Kebele. *Int. J. Res. Environ. Sci.* **2019**, *5*, 29–38. [[CrossRef](#)]
19. Worku, H. Environmental and Socioeconomic Impacts of Cobblestone Quarries in Addis Ababa and Implication for Resource Use Efficiency, Environmental Quality, and Sustainability of Land After-use. *Environ. Qual. Manag.* **2017**, *27*, 41–61. [[CrossRef](#)]
20. Tiberio Moilinga, P.; Robert Athian, M. Impacts of Stone Quarrying on Local Vegetation in Mount Korok Area, Juba, Central Equatoria State, South Sudan. In *New Insights Into Protected Area Management and Conservation Biology [Working Title]*; IntechOpen: London, UK, 2023.
21. Belay, L.; Birhane, E.; Zenebe, A.; Weldu, A.; Chiemela, S.N.; Solomon, N. Effects of Stone Mining on Woody Plant Species Diversity and Selected Soil Properties in Northern Ethiopia. *Environ Syst Res* **2020**, *9*, 12. [[CrossRef](#)]
22. Assefa, G.; Gebregziabher, A. Environmental Impact and Sustainability of Aggregate Production in Ethiopia. In *Sandy Materials in Civil Engineering-Usage and Management*; Nemati, S., Tahmoorian, F., Eds.; IntechOpen: London, UK, 2020; ISBN 978-1-78985-835-8.
23. Misra, A.K. Influence of Stone Quarries on Groundwater Quality and Health in Fatehpur Sikri, India. *Int. J. Sustain. Built Environ.* **2013**, *2*, 73–88. [[CrossRef](#)]
24. Wondimu, A. *Environmental and Social Impacts of Stone Quarrying Activities in Addis Ababa: In the Case of Bole Sub City, Oshe Locality*; Addis Ababa University: Addis Ababa, Ethiopia, 2021.
25. Mohsin, M.; Zhu, Q.; Naseem, S.; Sarfraz, M.; Ivascu, L. Mining Industry Impact on Environmental Sustainability, Economic Growth, Social Interaction, and Public Health: An Application of Semi-Quantitative Mathematical Approach. *Processes* **2021**, *9*, 972. [[CrossRef](#)]
26. Wassie, S.B. Natural Resource Degradation Tendencies in Ethiopia: A Review. *Environ Syst Res* **2020**, *9*, 33. [[CrossRef](#)]
27. Kidane, Y.O.; Hoffmann, S.; Jaeschke, A.; Beloiu, M.; Beierkuhnlein, C. Ericaceous Vegetation of the Bale Mountains of Ethiopia Will Prevail in the Face of Climate Change. *Sci. Rep.* **2022**, *12*, 1858. [[CrossRef](#)] [[PubMed](#)]
28. *Climate Change 2007: Impacts, Adaptation and Vulnerability: Contribution of Working Group II to the Fourth Assessment Report of the Intergovernmental Panel on Climate Change*; Groupe d'experts Intergouvernemental sur l'évolution du Climat (Ed.) Cambridge University Press: Cambridge, UK, 2007; ISBN 978-0-521-70597-4.
29. Mieke, G.; Mieke, S. *Ericaceous Forests and Heathlands in the Bale Mountains of South Ethiopia Ecology and Man's Impact*, 1st ed.; Traute Warnke Verlag, Reinbek: Hamburg, Germany, 1994; Volume 1, ISBN 3-9801591-4-0.
30. Sevara, C.; Verhoeven, G.; Doneus, M.; Draganits, E. Surfaces from the Visual Past: Recovering High-Resolution Terrain Data from Historic Aerial Imagery for Multitemporal Landscape Analysis. *J. Archaeol. Method Theory* **2018**, *25*, 611–642. [[CrossRef](#)]

31. Carabassa, V.; Domene, X.; Diaz, E.; Alcañiz, J.M. Mid-term Effects on Ecosystem Services of Quarry Restoration with Technosols under Mediterranean Conditions: 10-year Impacts on Soil Organic Carbon and Vegetation Development. *Restor. Ecol.* **2020**, *28*, 960–970. [CrossRef]
32. Rumsby, B.T.; Brasington, J.; Langham, J.A.; McLelland, S.J.; Middleton, R.; Rollinson, G. Monitoring and Modelling Particle and Reach-Scale Morphological Change in Gravel-Bed Rivers: Applications and Challenges. *Geomorphology* **2008**, *93*, 40–54. [CrossRef]
33. Rajakumari, S.; Mahesh, R.; Sarunjith, K.J.; Ramesh, R. Volumetric Change Analysis of the Cauvery Delta Topography Using Radar Remote Sensing. *Egypt. J. Remote Sens. Space Sci.* **2022**, *25*, 687–695. [CrossRef]
34. Davies, S.N.G.; Lai, L.W.C.; Chua, M.H. Seen from above: The Theoretical Future of Aerial Photos in Land Use, Environmental and Planning Study. *Land Use Policy* **2018**, *78*, 19–28. [CrossRef]
35. Đorđević, D.R.; Đurić, U.; Bakrač, S.T.; Drobnjak, S.M.; Radojčić, S. Using Historical Aerial Photography in Landslide Monitoring: Umka Case Study, Serbia. *Land* **2022**, *11*, 2282. [CrossRef]
36. Lu, L.; Zhou, Y.; Walker, R.T. Using Historical Aerial Photographs to Measure Earthquake Deformation: Testing the Effects of Scan Resolution. *Remote Sens. Environ.* **2021**, *252*, 112118. [CrossRef]
37. Schenk, T. Towards Automatic Aerial Triangulation. *ISPRS J. Photogramm. Remote Sens.* **1997**, *52*, 110–121. [CrossRef]
38. Eltner, A.; Sofia, G. Structure from Motion Photogrammetric Technique. In *Developments in Earth Surface Processes*; Elsevier: Amsterdam, The Netherlands, 2020; Volume 23, pp. 1–24. ISBN 978-0-444-64177-9.
39. Westoby, M.J.; Brasington, J.; Glasser, N.F.; Hambrey, M.J.; Reynolds, J.M. ‘Structure-from-Motion’ Photogrammetry: A Low-Cost, Effective Tool for Geoscience Applications. *Geomorphology* **2012**, *179*, 300–314. [CrossRef]
40. Arun, P.V. A comparative analysis of different dem interpolation methods. *Geod. Cartogr.* **2013**, *39*, 171–177. [CrossRef]
41. Yan, L.; Tang, X.; Zhang, Y. High Accuracy Interpolation of DEM Using Generative Adversarial Network. *Remote Sens.* **2021**, *13*, 676. [CrossRef]
42. Franke, R. Smooth Interpolation of Scattered Data by Local Thin Plate Splines. *Comput. Math. Appl.* **1982**, *8*, 273–281. [CrossRef]
43. Hutchinson, M.F. Calculation of Hydrologically Sound Digital Elevation Models. In *Proceedings of the Third International Symposium on Spatial Data Handling*, Sydney, Australia, 17 August 1988; pp. 117–133.
44. Philip, G.M.; Watson, D.F. A precise method for determining contoured surfaces. *APPEA J.* **1982**, *22*, 205. [CrossRef]
45. Riquelme, A.; Del Soldato, M.; Tomás, R.; Cano, M.; Jordá Bordehore, L.; Moretti, S. Digital Landform Reconstruction Using Old and Recent Open Access Digital Aerial Photos. *Geomorphology* **2019**, *329*, 206–223. [CrossRef]
46. Schaffrath, K.R.; Belmont, P.; Wheaton, J.M. Landscape-Scale Geomorphic Change Detection: Quantifying Spatially Variable Uncertainty and Circumventing Legacy Data Issues. *Geomorphology* **2015**, *250*, 334–348. [CrossRef]
47. James, L.A.; Hodgson, M.E.; Ghoshal, S.; Latiolais, M.M. Geomorphic Change Detection Using Historic Maps and DEM Differencing: The Temporal Dimension of Geospatial Analysis. *Geomorphology* **2012**, *137*, 181–198. [CrossRef]
48. Khan, S.; Bartley, R.; Kinsey-Henderson, A.; Hawdon, A. Application of Multi Temporal Lidar Dems for Tracking Gully Rehabilitation Efforts in Highly Erosive Landscapes of the Burdekin Catchment, Queensland, Australia. *SSRN J.* **2022**. [CrossRef]
49. Azmoon, B.; Biniyaz, A.; Liu, Z. Use of High-Resolution Multi-Temporal DEM Data for Landslide Detection. *Geosciences* **2022**, *12*, 378. [CrossRef]
50. Kidane, Y.O.; Steinbauer, M.J.; Beierkuhnlein, C. Dead End for Endemic Plant Species? A Biodiversity Hotspot under Pressure. *Glob. Ecol. Conserv.* **2019**, *19*, e00670. [CrossRef]
51. Alvis, C. *History of 1370th Photo Mapping Wing (Interim Report of Field Operation from January 1, 1964-June 30, 1964)*; Volume II of II; Turner AFB: Albany, GA, USA, 1979.
52. Muhammed, M.A.; Hailu, B.T.; Mieke, G.; Nauss, T.; Zeuss, D. High-Resolution Digital Elevation Models and Orthomosaics Generated from Historical Aerial Photographs (since the 1960s) of the Bale Mountains in Ethiopia, Zenodo [data set]. 2022. Available online: <https://zenodo.org/records/7271617> (accessed on 23 March 2024).
53. Bangen, S.G.; Wheaton, J.M.; Bouwes, N.; Bouwes, B.; Jordan, C. A Methodological Intercomparison of Topographic Survey Techniques for Characterizing Wadeable Streams and Rivers. *Geomorphology* **2014**, *206*, 343–361. [CrossRef]
54. Idris, M. Evaluation of GPS-RTK and Total Station for Topographic Survey and Strategic Decision in Private Companies. In *Proceedings of the 1st International Conference on Geodesy, Geomatics, and Land Administration 2019*; pp. 323–332. Available online: <https://knepublishing.com/index.php/KnE-Engineering/article/view/5874> (accessed on 23 March 2024).
55. Belmonte, A.A.; Biong, M.M.P.; Macatulad, E.G. Dem generation from close-range photogrammetry using extended python photogrammetry toolbox. *Int. Arch. Photogramm. Remote Sens. Spat. Inf. Sci.* **2017**, *XLII-4/W5*, 11–19. [CrossRef]
56. Carrivick, J.; Smith, M.; Quincey, D. *Structure from Motion in the Geosciences*; John Wiley & Sons, Ltd.: Hoboken, NJ, USA, 2016; ISBN 978-1-118-89584-9.
57. ESRI Inc. *ArcGIS Desktop, Release 10, Environmental Systems Research Institute [Software]*; ESRI Inc.: Redlands, CA, USA, 2021.
58. Bailey, P.; Wheaton, J.; Reimer, M.; Brasington, J. Geomorphic Change Detection Software Version 7.5.0. Zenodo [software]. , 2020. Available online: <https://zenodo.org/records/7248344> (accessed on 10 September 2023).
59. Snavely, N.; Seitz, S.M.; Szeliski, R. Modeling the World from Internet Photo Collections. *Int. J. Comput. Vis.* **2008**, *80*, 189–210. [CrossRef]
60. Eltner, A.; Kaiser, A.; Castillo, C.; Rock, G.; Neugirg, F.; Abellán, A. Image-Based Surface Reconstruction in Geomorphometry—Merits, Limits and Developments. *Earth Surf. Dynam.* **2016**, *4*, 359–389. [CrossRef]

61. AgiSoft LLC Agisoft Metashape Professional, Version 1.8.0.13794 45 [software], St. Petersburg. 2021. Available online: <https://www.agisoft.com/downloads/installer/> (accessed on 7 September 2023).
62. Lowe, D.G. Object Recognition from Local Scale-Invariant Features. In Proceedings of the Proceedings of the Seventh IEEE International Conference on Computer Vision, Kerkyra, Greece, 20–27 September 1999; IEEE: Kerkyra, Greece, 1999; Volume 2, pp. 1150–1157.
63. Šiljeg, A.; Lozić, S.; Šiljeg, S. A Comparison of Interpolation Methods on the Basis of Data Obtained from a Bathymetric Survey of Lake Vrana, Croatia. *Hydrol. Earth Syst. Sci.* **2015**, *19*, 3653–3666. [[CrossRef](#)]
64. Rishikeshan, C.A.; Katiyar, S.K.; Mahesh, V.N.V. Detailed Evaluation of DEM Interpolation Methods in GIS Using DGPS Data. In Proceedings of the 2014 International Conference on Computational Intelligence and Communication Networks, Bhopal, India, 14–16 November 2014; IEEE: Bhopal, India, 2014; pp. 666–671.
65. Ajvazi, B.; Czimber, K. A Comparative Analysis of Different Dem Interpolation Methods in Gis: Case Study of Rahovec, Kosovo. *Geod. Cartogr.* **2019**, *45*, 43–48. [[CrossRef](#)]
66. Oliver, M.A.; Webster, R. Kriging: A Method of Interpolation for Geographical Information Systems. *Int. J. Geogr. Inf. Syst.* **1990**, *4*, 313–332. [[CrossRef](#)]
67. Habib, M.; Alzubi, Y.; Malkawi, A.; Awwad, M. Impact of Interpolation Techniques on the Accuracy of Large-Scale Digital Elevation Model. *Open Geosci.* **2020**, *12*, 190–202. [[CrossRef](#)]
68. Wheaton, J.M.; Brasington, J.; Darby, S.E.; Sear, D.A. Accounting for Uncertainty in DEMs from Repeat Topographic Surveys: Improved Sediment Budgets. *Earth Surf. Process. Landf.* **2010**, *35*, 136–156. [[CrossRef](#)]
69. Groos, A.R.; Niederhauser, J.; Wraase, L.; Hänsel, F.; Nauss, T.; Akçar, N.; Veit, H. The Enigma of Relict Large Sorted Stone Stripes in the Tropical Ethiopian Highlands. *Earth Surf. Dynam.* **2021**, *9*, 145–166. [[CrossRef](#)]
70. Rault, C.; Dewez, T.J.B.; Aunay, B. Structure-from-motion processing of aerial archive photographs: Sensitivity analyses pave the way for quantifying geomorphological changes since 1978 in la réunion island. *ISPRS Ann. Photogramm. Remote Sens. Spat. Inf. Sci.* **2020**, *V-2-2020*, 773–780. [[CrossRef](#)]
71. James, M.R.; Robson, S. Straightforward Reconstruction of 3D Surfaces and Topography with a Camera: Accuracy and Geoscience Application. *J. Geophys. Res.* **2012**, *117*, 2011JF002289. [[CrossRef](#)]
72. Barrand, N.E.; Murray, T.; James, T.D.; Barr, S.L.; Mills, J.P. Optimizing Photogrammetric DEMs for Glacier Volume Change Assessment Using Laser-Scanning Derived Ground-Control Points. *J. Glaciol.* **2009**, *55*, 106–116. [[CrossRef](#)]
73. Garnero, G.; Godone, D. Comparisons between Different Interpolation Techniques. *Int. Arch. Photogramm. Remote Sens. Spatial Inf. Sci.* **2014**, *XL-5/W3*, 139–144. [[CrossRef](#)]
74. Zimmerman, D.; Pavlik, C.; Ruggles, A.; Armstrong, M.P. An Experimental Comparison of Ordinary and Universal Kriging and Inverse Distance Weighting. *Math. Geol.* **1999**, *31*, 375–390. [[CrossRef](#)]
75. Karuppasamy, S.; Kaliappan, S.; Karthiga, R.; Divya, C. Surface Area Estimation, Volume Change Detection in Lime Stone Quarry, Tirunelveli District Using Cartosat-1 Generated Digital Elevation Model (DEM). *CS* **2016**, *7*, 849–858. [[CrossRef](#)]
76. Tyc, G.; Tulip, J.; Schulten, D.; Krischke, M.; Oxfort, M. The RapidEye Mission Design. *Acta Astronaut.* **2005**, *56*, 213–219. [[CrossRef](#)]

**Disclaimer/Publisher’s Note:** The statements, opinions and data contained in all publications are solely those of the individual author(s) and contributor(s) and not of MDPI and/or the editor(s). MDPI and/or the editor(s) disclaim responsibility for any injury to people or property resulting from any ideas, methods, instructions or products referred to in the content.